Strain hardening by sediment transport – Supplementary Information

Fernando D. Cúñez and Erick M. Franklin

School of Mechanical Engineering,

UNICAMP - University of Campinas,

Rua Mendeleyev, 200,

Campinas, SP, Brazil

Morgane Houssais

Levich Institute, City College of New York - CUNY

140th Street and Convent Avenue,

NewYork, NY 10031, USA

Paulo Arratia

Mechanical Engineering and Applied Mechanics,

University of Pennsylvania,

Philadelphia, 19104,

Pennysylvania, USA

Douglas J. Jerolmack

Department of Earth and Environmental Science,

and Mechanical Engineering and Applied Mechanics,

University of Pennsylvania,

Philadelphia, 19104,

Pennysylvania, USA

(Dated: August 30, 2021)

ABSTRACT

This file contains supplementary information of two general types: additional detail on experimental techniques and analytical methods; and supplementary data figures that support the conclusions reported in the main text. We describe and illustrate how experimental quantities such as particle velocity, concentration, and strain were derived from raw images — the principle data product of our study. We then present results of strain hardening and hysteresis for a variety of experiments, showing how our findings are qualitatively similar to those described in the main text under a range of conditions. Finally, this file includes a table showing all experimental conditions explored in the study.

DETERMINING PARTICLE VELOCITY AND VOLUME FRACTION

We examined a region of the sediment bed that is 1920 px in the horizontal (x) direction and 960 px in the vertical (z) direction, corresponding to 48.5 mm $\times$ 24.23 mm. Images were obtained at the channel centerline (Fig. 1 (a)) at a rate of 60 Hz. We first computed spatially-resolved (two-dimensional, 2D) "instantaneous" velocity measurements from successive image pairs by performing Particle Image Velocimetry (PIV) using PIV-LAB [1, 2],with an interrogation area of 64 px $\times$ 64 px and an overlap of 50%. This corresponds to 60^2 interrogation areas, and a spatial resolution of 0.8 mm $\times$ 0.8 mm. Figure 1 shows an example of the obtained velocities for the region of interest. Average profiles of velocity with depth, determined for each stress cycle, were then computed by $x-$averaging all instantaneous velocity measurements and then time-averaging all $x - averaged$ values over the 10-min duration of a stress cycle (Fig. 1).

To estimate the particle volume fraction in 2D, we first detected all particles in each image using the method presented by Houssais *et al.* [3]. Profiles of 2D volume (area) fraction for each depth z were then computed from the area occupied by the detected particles in each x strip, averaged in time over the duration of each stress cycle.

DETERMINING STRAIN AND STRAIN RATE

Strain was determined for each pixel in the area of interest of a fixed duration of the stress cycle, $\Delta t = 600s$. We examined the change in pixel intensity inside image strips of

width L_x and height d, a quantity we call mobility m $[px^2]$. If one particle of diameter d moves laterally in that strip over a distance $\Delta x = d$ – which corresponds to the case where the strain $\varepsilon = \Delta x/\Delta z = 1$ – then $m = 2\pi(d/2)^2$ $[px^2]$. In the case of n particles in a dense configuration that move along a strip of lateral size L_x, it should be the case that $L_x = n * d$. We now define the dimensionless parameter $m^* = m\ (scale)^2/\pi(d/2)^2$, where *scale* is the resolution [m/pxl] in the image. For the case of one particle exhibiting $\epsilon = 1$, $m^* = 2$. For the case of n particles in the dense configuration described above, $m^* = 2n = 2L_x/d$. This case is the largest deformation that can be monitored by measuring pxl change; when $\varepsilon > 1$, some particle displacement is not captured. We therefore determine a saturation value of the mobility measurement as $m^*_{sat} = 2L_x/d$; for our images, $m^*_{sat} = 64.5$ (Fig. 3).

Using the time-averaged concentration profile $\langle C(z)\rangle\,(z)$, we define the local and time-averaged measurement of strain, over a duration $\Delta t = 600s$, and for $m^* < m^*_{sat}$, as:

$$\langle \varepsilon(z)\rangle = \frac{C_{sat}}{\langle C(z)\rangle}\frac{d}{2Lx}m^*(z) \tag{1}$$

where m $[px^2]$ comes from the absolute difference between two images. To obtain the m profiles at each time step, we compared the first image of each cycle with the next ones until $t = 600s$, i.e., $m(t) = abs(image(1) - image(t))$. The average strain value in the creep regime is given by the expression:

$$\varepsilon_{creep} = \frac{1}{z_c}\int_0^{z_c} \langle \varepsilon(z)\rangle\, dz \tag{2}$$

where z_c is the depth associated with the kink in the mean velocity profile, that separates the creep and dense-flow regimes [3]. The average strain value in the flowing regime is given by:

$$\varepsilon_{flow} = \frac{1}{z|_{m^*=m^*_{sat}} - z_c}\int_{z_c}^{z|_{m^*=m^*_{sat}}} \langle \varepsilon(z)\rangle\, dz \tag{3}$$

where $z|_{m^*=m^*_{sat}}$ is the depth of the bed where m^* reaches m^*_{sat}. Finally, the total average strain follows the expression:

$$\varepsilon_T = \frac{1}{z|_{m^*=m^*_{sat}}}\int_0^{z|_{m^*=m^*_{sat}}} \langle \varepsilon(z)\rangle\, dz \tag{4}$$

[1] W. Thielicke and E. Stamhuis, Journal of open research software **2** (2014).

[2] W. Thielicke, Diss. University of Groningen (2014).

[3] M. Houssais, C. P. Ortiz, D. J. Durian, and D. J. Jerolmack, Nat. Commun. **6** (2015).

SUPPLEMENTARY FIGURES

TABLE I: Tested conditions. From left to right, the test number, Shields number normalized by its critical value, lid velocities at the channel centerline, number of cycles, shear direction during the preparation of the bed, shear direction during cycles, and direction of the last cycle. OBS: for test 6, $\theta/\theta_c = 4$ in the last cycle.

Test	θ/θ_c	U_{lid}	number of cycles	preparation	cycles	last cycle
...	...	mm/s	...	...	...	...
1	1	9	7	Same direction	Same direction	Reversed direction
2	2	19	8	Same direction	Same direction	Reversed direction
3	3	28	9	Same direction	Same direction	Reversed direction
4	4	37	11	Same direction	Same direction	Reversed direction
5	5	46	11	Same direction	Same direction	Reversed direction
6	2	19	8	Same direction	Same direction	Same direction
7	2	19	8	Reversed direction	Same direction	Reverse
8	2	19	8	Same direction	Alternating direction	Reverse
9	$1-5-1$	$9-46$	13	Same direction	Same direction	Same direction
10	$5-1-5$	$46-9$	13	Same direction	Same direction	Same direction

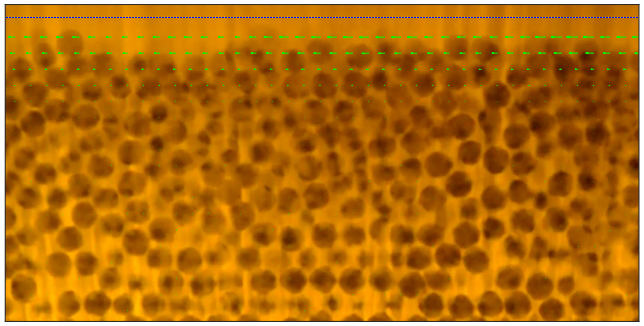

(a)

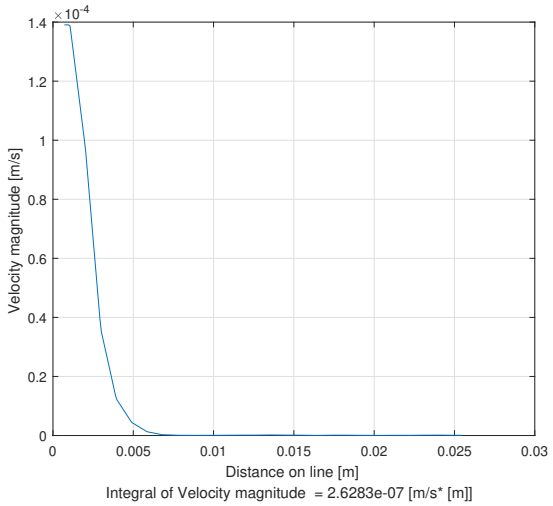

(b)

FIG. 1: Cross-correlation of sequential images to determine velocity, using PIV-LAB: (a) Example of "instantaneous" velocities obtained from PIV-LAB; and (b) averaged velocity profile.

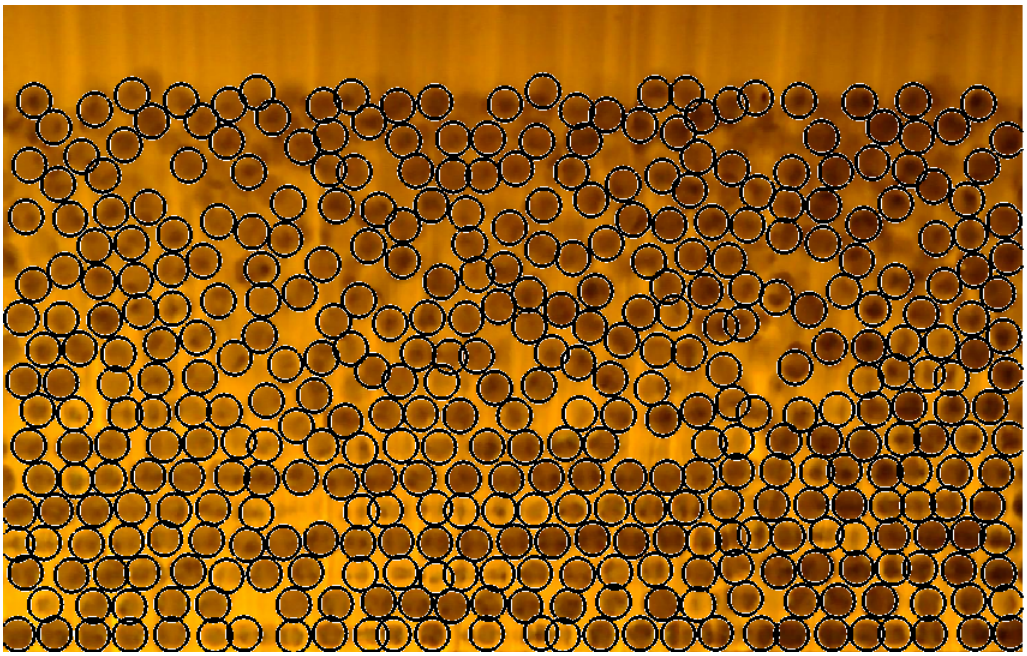

FIG. 2: Example image showing detection of particles, using the method described in Houssais *et al.* [3].

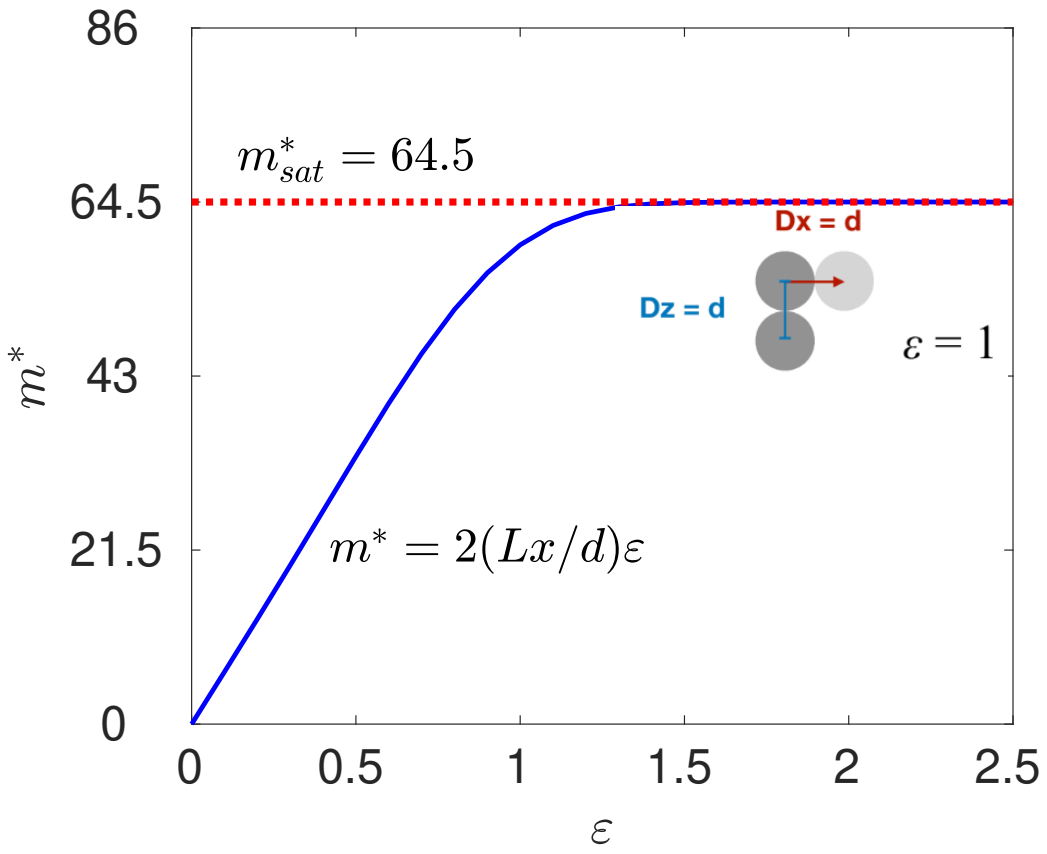

FIG. 3: Dimensionless mobility as a function of strain, showing saturation at a strain of 1 that defines our measurement limit.

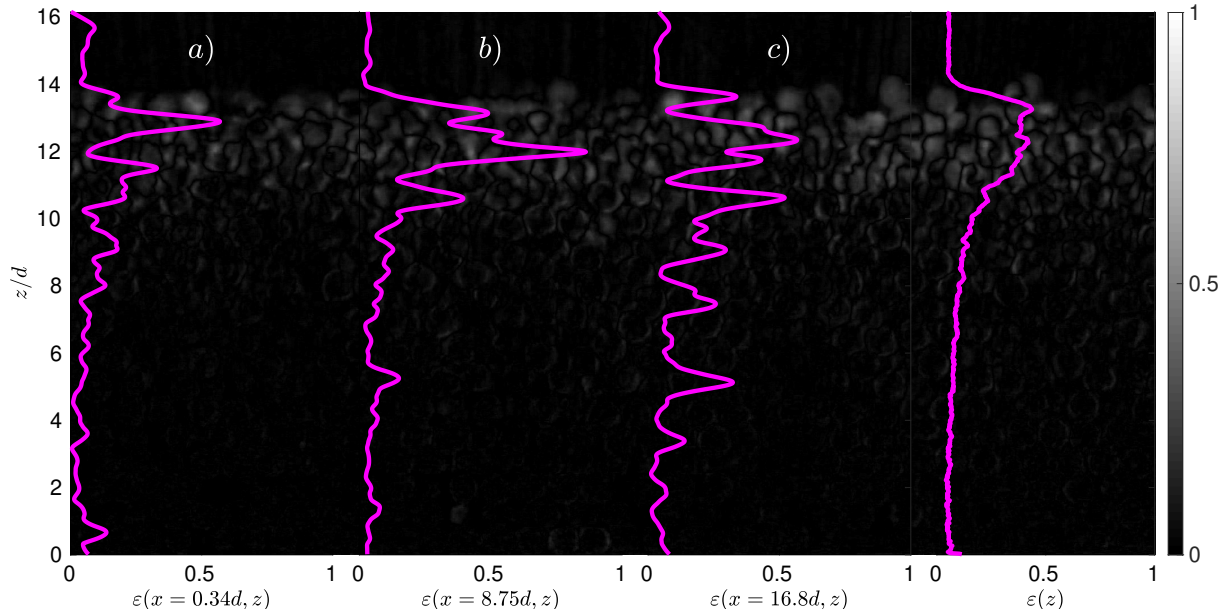

FIG. 4: Local and spatially-averaged strain measurements. Background shows local strain measurements for each pixel.Profiles are superimposed for strain as a function of depth, $\varepsilon(z)$, at different locations x in the image, for an experiment with $\theta/\theta_c = 2$ at the last stress cycle and at time $t = 600s$. Strain profiles at (a) location $x = 0.34d$, (b) location $x = 8.75d$, (c) location $x = 16.8d$, and (d) averaged spatially across all locations x.

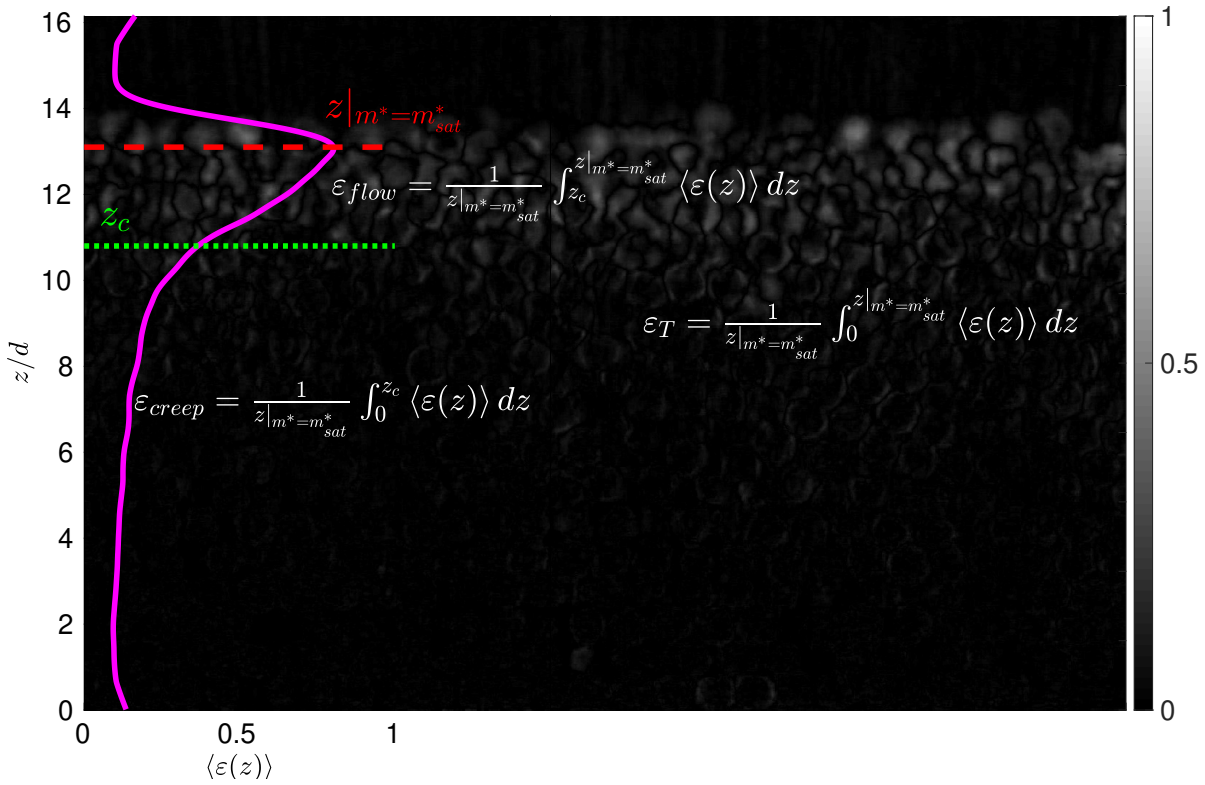

FIG. 5: Local and time-averaged strain for different regimes for $\theta/\theta_c = 2$, computed over the last stress cycle. Equations used to determine strain for Creep, Flowing and Total (Creep + Flowing) are shown.

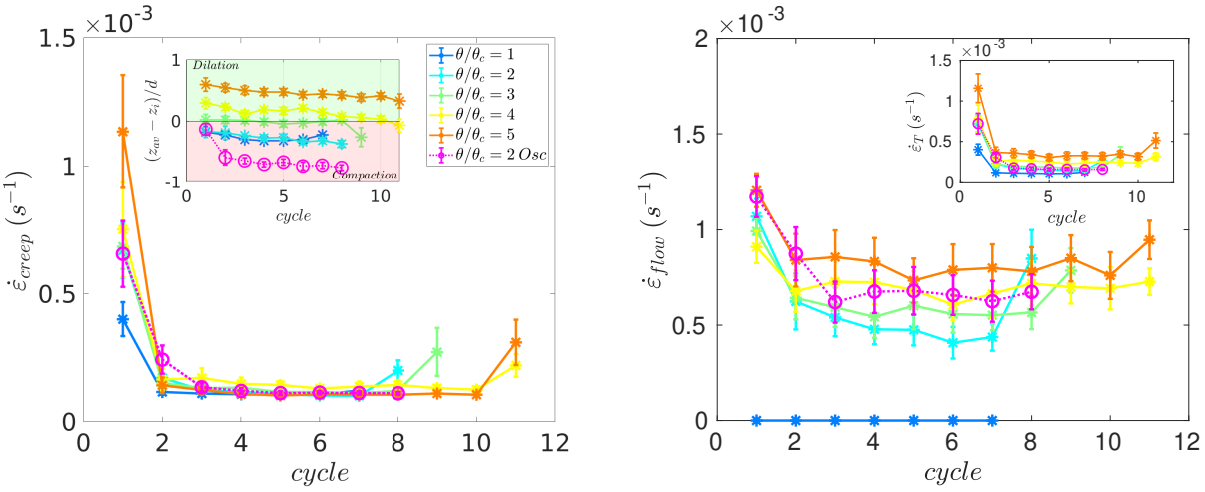

(a) (b)

FIG. 6: (a) Strain rate in the creeping regime as a function of the number of stress cycles, for uni-directional experiments where shear direction was reversed only for the last cycle; inset shows the height of the sediment bed, determined as described in the main text. (b) Strain rate in the flowing regime as a function of the number of cycles; inset shows the total strain rate. Data presented for tests 1-5 and 8 in Table I); legend in (a) indicates associated stress.

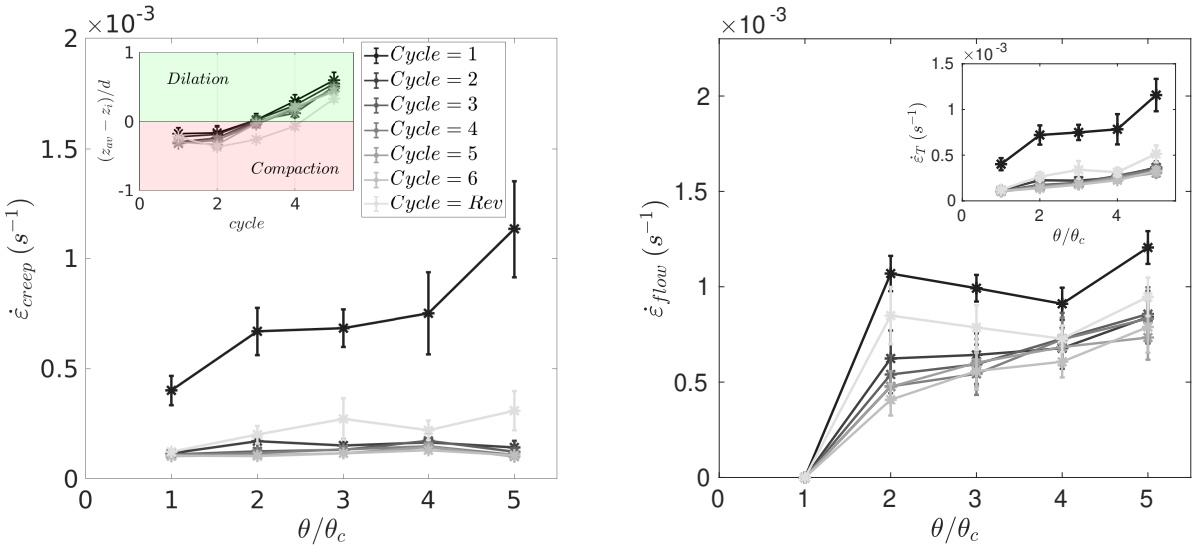

(a) (b)

FIG. 7: An alternative way to present the data in Figure 6; strain rate as a function of the applied shear stress, where grayscale corresponds to the stress cycle. (a) Strain rate for the creeping regime; and (b) strain rate for the flowing regime. Insets follow Figure 6; results shown for tests 1-5 in Tab.I.

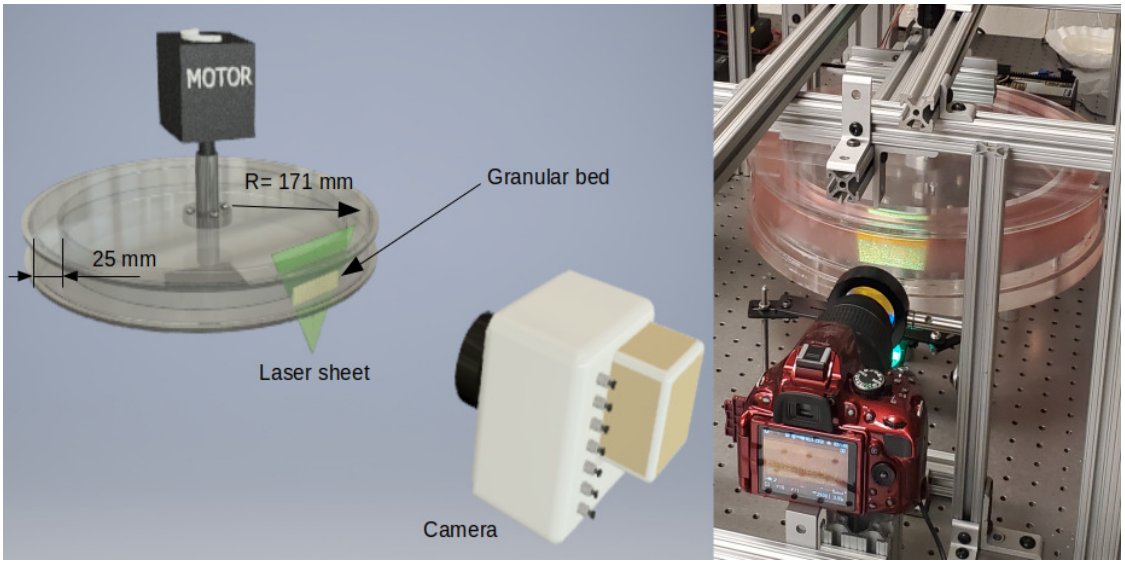

FIG. 8: A layout (on the left) and a photograph (on the right) of the experimental setup.

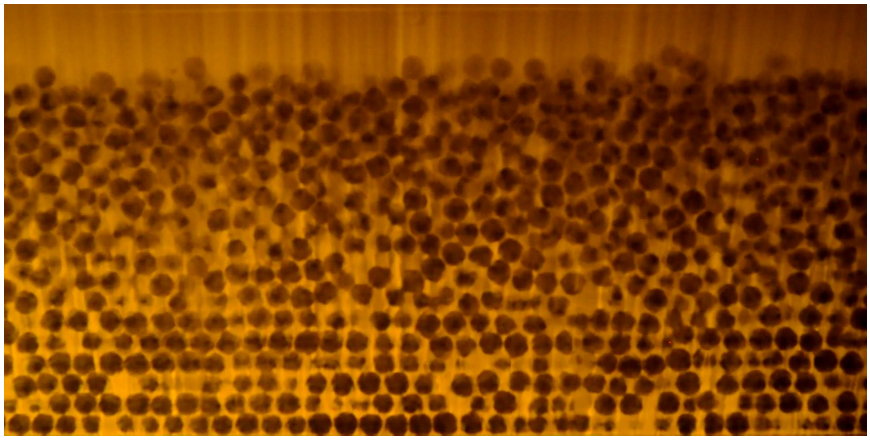

FIG. 9: Raw image of the grains within the bed in the laser plane.

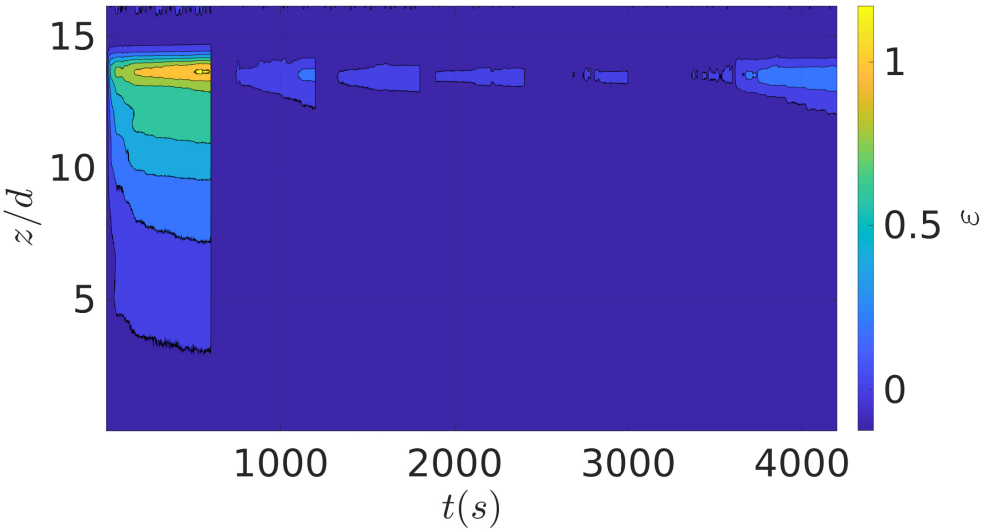

FIG. 10: M matrix representing local particles' mobility intensity for test 1 (all cycles included) with reversal at the last cycle. Variation from blue (darker shades in grayscale) to yellow (brighter shades in grayscale) corresponds to increasing in mobility..

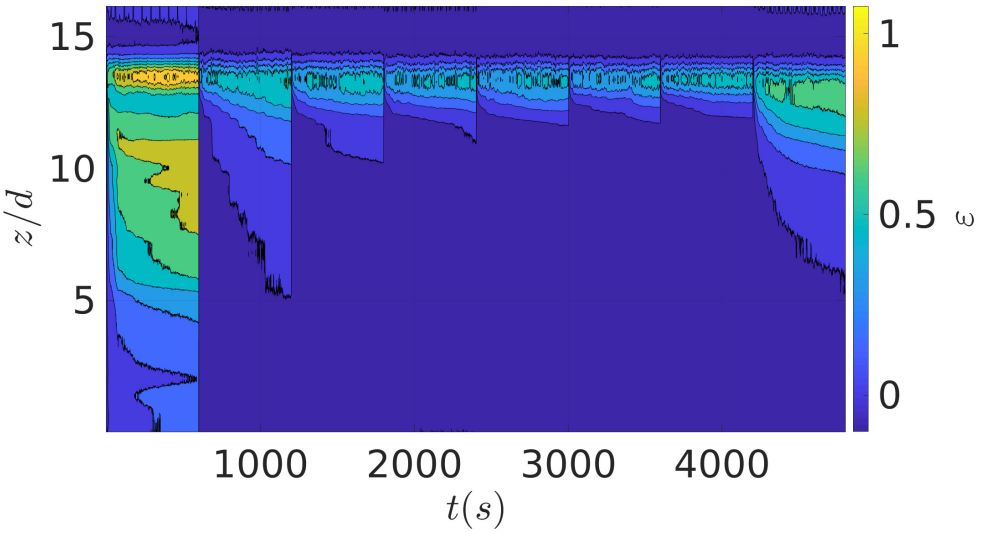

FIG. 11: Same as Figure 10, but for test 2 (all cycles included).

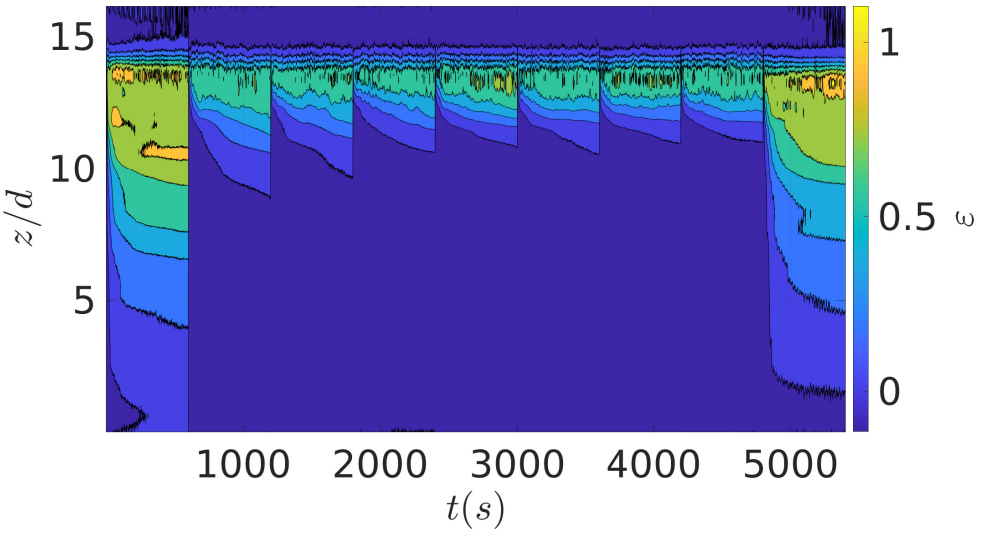

FIG. 12: Same as Figure 10, but for test 3 (all cycles included)

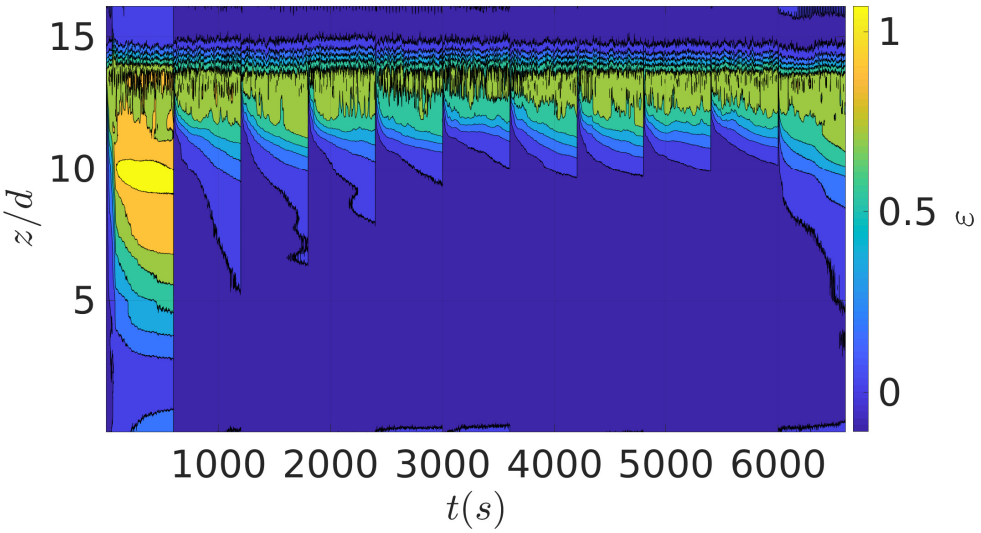

FIG. 13: Same as Figure 10, but for test 4 (all cycles included)

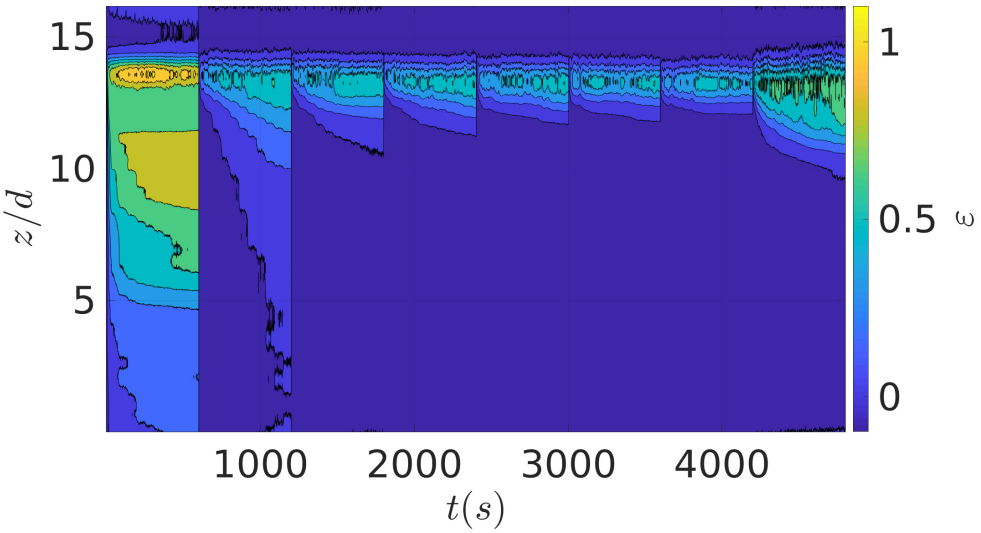

FIG. 14: Same as Figure 10, but for test 6 (all cycles included)

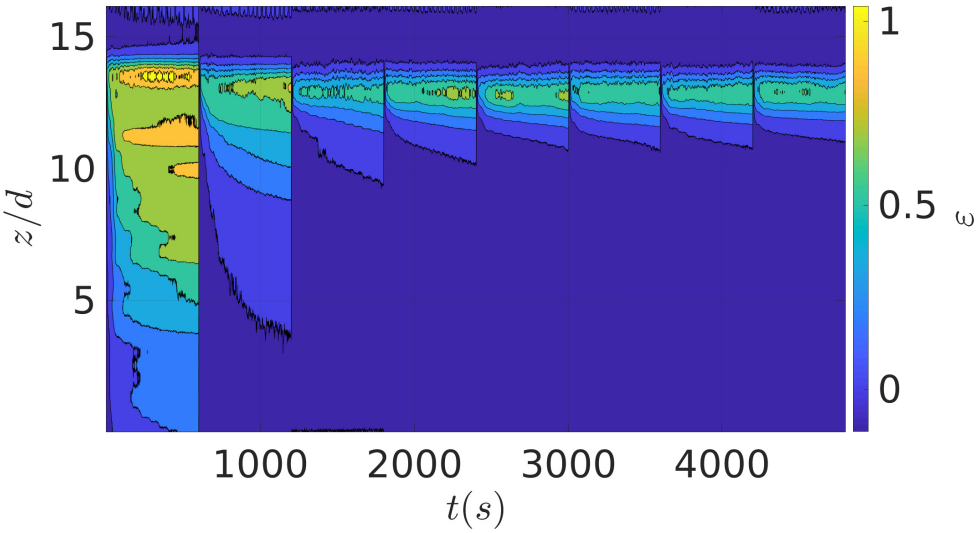

FIG. 15: Same as Figure 10, but for test 8 (all cycles included)